# Proton-induced deuteron breakup at 156 MeV

J. P. Didelez, I. D. Goldman,* E. Hourany,† H. Nakamura,‡ F. Reide, and T. Yuasa
*Institut de Physique Nucléaire, Université de Paris-Sud, 91-Orsay, France*
(Received 3 December 1973)

The $^2H(p, 2p)n$ and $^2H(p, pn)p$ reactions have been investigated simultaneously using the 156 MeV synchrocyclotron beam. Outgoing nucleons were detected in coincidence by a NaI detector and a large liquid scintillation counter providing energy–time-of-flight–biparametric spectra from which the threefold differential cross sections $d^3\sigma/d\Omega_1 d\Omega_2 dE_1$ are deduced. For suitable angle pairs, the experimental spectra show either the characteristic quasi-free scattering peak, or the $p$-$p$ or $p$-$n$ final state interaction peaks. The experimental results are compared with various theoretical predictions; i.e., a simple spectator model calculation, off-energy-shell calculations including first and second order terms of a multiple scattering series, with or without the Coulomb interaction, and an extension to intermediate energy of a Amado type model. These theoretical calculations are briefly discussed.

[NUCLEAR REACTIONS $(d^3\sigma/d\Omega_1 d\Omega_2 dE_1)_{exp}$ for $^2H(p, 2p)$ and $^2H(p, pn)$ reactions at 156 MeV. Studies of $p$-$n$ and $p$-$p$ final state interactions. The comparison with some theoretical approximate calculations discussed.]

## I. INTRODUCTION

Since Faddeev published for the first time the theory of nonrelativistic three-particle systems,[1] the study of three-particle systems has progressed rapidly in both the theoretical and experimental domains. However, at the present stage, some approximations have to be made in order to numerically solve these equations. One of the approximations is the use of separable potentials for the two-nucleon interactions. Following the pioneer work of Aaron, Amado, and Yam,[2] many numerical calculations have been performed for the three-nucleon systems at low energy ($E \leq 40$ MeV) where $S$-wave states are dominant.[3-5] For higher energies, difficulties arise from the fact that the separable two-body interactions usually employed cease to provide a realistic description of the observable two nucleon process. Wallace[6] has attempted to apply the exact three-body formalism in a reasonable manner at higher energies ($E \leq 100$ MeV) employing separable potentials.

Another approximation, the "impulse approximation," is usually used for the higher energies. Since the work of Chew[7] and Chew and Wick[8] using this approximation to interpret the nucleon-deuteron scattering for $E \geq 100$ MeV, the impulse approximation for the $p$-$d$ scattering has been improved by several authors from a simple spectator model to more elaborate ones.[9-11] The spectator model and the simple impulse approximation neglect the effects of multiple scattering, final state interactions, and off-energy-shell effects. These effects have been considered by Everett[9] and Cromer, Cromer, and Thorndike[10] for the deuteron breakup reaction by a proton, and by Benoist-Gueutal *et al.*[11] for $p$-$d$ elastic scattering.

Since then, L'Huillier,[12] Brown and Thorndike,[13] and Sakamoto, Takeutchi, and one of the present authors (T. Y.)[14] have also treated the breakup of the deuteron by the $(p, 2p)$ reaction within the framework of the impulse approximation, by introducing the final state interactions of nucleons in the $s$-waves[12,13] or in the $s, p$, and $d$ waves,[14] and taking into account the first and second order terms in the two-nucleon multiple scattering series development of the three-nucleon $t$ matrix. The calculations have been done with on energy-shell $T$ matrices.[12-14]

These calculations have shown the necessity of taking into account the effects of the multiple scattering and pointed out the possibility of final state interaction contributions. However, the agreement of these calculations with the experimental results of the $^2H(p, 2p)n$ reaction at 156 MeV[15,16] and at 198 MeV[13] is not quite satisfactory, even for some quasi-free scattering kinematic conditions.

Very recently, Ballot and L'Huillier have calculated the off-energy-shell two-nucleon $t$ matrices for the nucleon-nucleon scattering states and the $S$ and $D$ states of the deuteron using various local realistic potentials, in order to calculate the first and second order terms in the two-nucleon multiple scattering series development of the three-nucleon scattering amplitudes. A part of their program has been used by Morlet *et al.*[17] to compare with their recent experimental results obtained for the $^2H(p, 2p)n$ reaction at

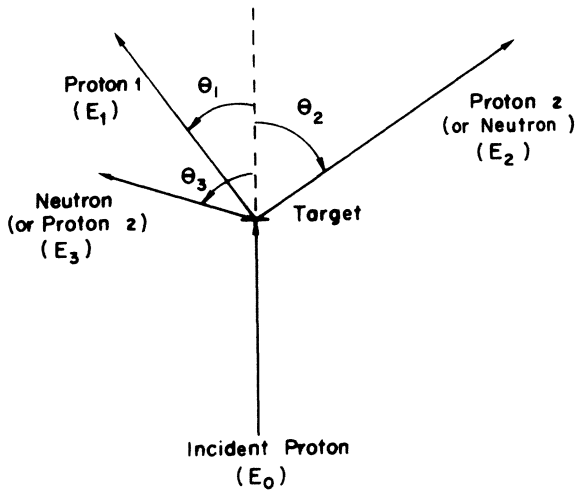


FIG. 1. Designation of kinematic parameters in the present experiment.

156 MeV.

Given such a status of theoretical and experimental studies of the deuteron breakup by intermediate energy protons, the quasi-free scattering (QFS) and the final state interactions (FSI) seem to be qualitatively interpreted, but still new information is needed for a deeper understanding of the reaction.

The simultaneous experimental study of the $^2H(p,2p)n$ and $^2H(p,pn)p$ reactions in the FSI regions might allow the observation of pronounced $p$-$n$ and $p$-$p$ final state interactions as has been seen at lower energy.[27] The comparison of the cross sections of both reactions over an extended range of kinematical conditions should provide information which will be helpful in understanding the problems associated with the theoretical treatment of quasi-free scattering and final state interactions. The new improvement of the theory by L'Huillier and Ballot of our Institute gave us the motivation for performing such an experiment employing a neutron detector specially developed for this purpose.

In Sec. 2, the choice of our kinematic conditions is presented, and in Sec. 3, the experimental procedure is described. In Sec. 4, the treatment of the experimental data and the experimental cross sections are given. Section 5 provides a brief description of the theoretical calculations and the comparison of the calculated results with our experimental results. Section 6 contains the conclusions.

## II. KINEMATIC CONDITIONS

In the present experiment, two of the outgoing nucleons were detected at fixed angles by measuring the energy of one proton and the time of flight of the second nucleon (a proton or a neutron).

TABLE I. The kinematic conditions chosen for the quasi-free and final state interaction studies.

| Interested region | $\theta_1$ (deg) | $\theta_2$ (deg) | $\theta_3$ (deg) | $E_1$ (MeV) | $E_2$ (MeV) | $E_3$ (MeV) | $E_{1-3}^{rel}$ (MeV) | $E_{2-3}^{rel}$ (MeV) |
|---|---|---|---|---|---|---|---|---|
| QFS | 52.5 | −35 | 1.04 | Peak 53.60 | 100.17 | 0.0041 | 54.617 | 104.599 |
| | | | (4.94 [a]) | (53.60) | (100.17) | (0.0035) | (54.544) | (104.440) |
| | 42.5 | −45 | 3.55 | Peak 80.20 | 73.57 | 0.0055 | 82.698 | 75.708 |
| | | | (−6.58) | (80.40) | (73.37) | (0.0049) | (83.0089) | (75.1747) |
| FSI | | | | QFS | | | | |
| | 45 | −57 | −2.24 | Peak 88.20 | 62.20 | 3.3714 | 71.8540 | 50.7182 |
| | | | (−2.09) | (88.20) | (62.41) | (3.3636) | (71.2338) | (51.0787) |
| | | | | FSI | | | | |
| | | | 49.05 | Peak 31.00 | 91.6336 | 31.1402 | 0.1571 | 158.4200 |
| | | | (49.04) | (31.00) | (91.5812) | (31.1926) | (0.1607) | (158.1831) |
| | | | | QFS | | | | |
| | 48 | −55 | −1.39 | Peak 82.40 | 67.38 | 3.9915 | 65.9737 | 54.0581 |
| | | | (−1.25) | (82.40) | (67.39) | (3.9825) | (65.8197) | (53.9779) |
| | | | | FSI | | | | |
| | | | 48.70 | Peak 29.40 | 94.86 | 29.52 | 0.0045 | 155.6743 |
| | | | (48.74) | (29.40) | (94.81) | (29.57) | (0.0052) | (155.4400) |

[a] The values in parentheses are for the ($p$, $pn$) reactions.

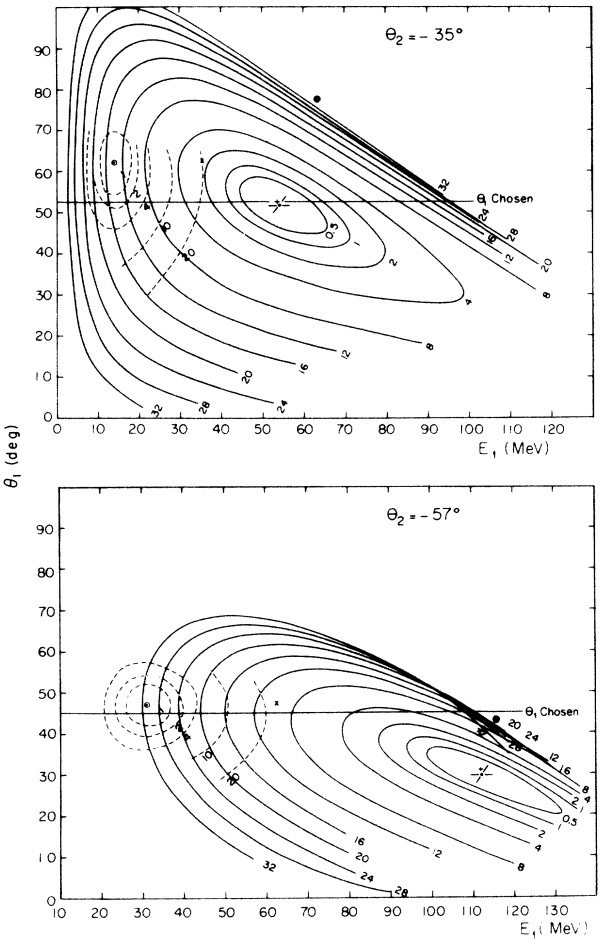


FIG. 2. Maps of the iso-$E_3$ (solid line) and iso-$E_{1-3}^{rel}$ (dashed line) curves (where the energies are indicated in MeV), with the chosen kinematic conditions. The locations of $p$ and $d$ peaks due to $p$-$d$ elastic scattering and the $p$ peak due to $p$-$H$ scattering are also figured by the ⊙, ×, and ⟩···⟨, respectively. (a) kinematic conditions including the QFS peak at $\theta_1 = 52.5°$ and $\theta_2 = -35°$; (b) kinematic conditions including the FSI peak at $\theta_1 = 45°$ and $\theta_2 = -57°$.

The scattering angles and the kinematic energies in the laboratory system of three nucleons in the final state are designated by $\theta_1$, $\theta_2$, and $\theta_3$ and $E_1$, $E_2$, and $E_3$, respectively. The solid angles of detection corresponding to $\theta_1$ and $\theta_2$ are designated by $\Delta\Omega_1$ and $\Delta\Omega_2$ (see Fig. 1). We made two series of experiments. In the first one, various pairs of angles were chosen, more or less arbitrarily, to survey the general behavior of the $^2H(p,2p)n$ and $^2H(p,pn)p$ reactions. In the second series we were interested especially in the study of the quasi-free scattering and the final state interaction regions.

For the second series we have chosen two pairs of the scattering angles $\theta_1 - \theta_2$ in which the spectra as a function of $E_1$ contain the quasi-free scattering peaks ($E_3 \sim 0$), and another two pairs in which the final state interactions between the first and the third nucleons should be strong. (A relative energy between the first and the third nucleons, $E_{1-3}^{rel} \sim 0$ is kinematically allowed.) The $\theta_1 - \theta_2$ pairs selected for the study of the quasi-free and final state interaction processes in the second series are presented in Table I. The relevant kinematic information for these angles is indicated in Fig. 2 in which the iso-$E_3$ curves (continuous lines) and the iso-$E_{1-3}^{rel}$ curves (dotted lines) are drawn. (The numbers written on curves correspond to energies in MeV.) Also indicated in Fig. 2 are the locations of the $p$ and $d$ peaks arising from $p$-$d$ elastic scattering and the $p$ peak arising from $p$-H scattering.

For the $^2H(p,2p)n$ reaction in the kinematic conditions corresponding to quasi-free scattering, there always exists a contribution due to $p$-$p$ elastic scattering from the hydrogen impurity in the deuterium target. For the kinematic conditions corresponding to the final state interaction peak, the tail of the $p$-$d$ elastic scattering peak arising from nuclear reactions in the NaI detector could obscure the final state interaction peak. In spite of these difficulties, we have chosen the $\theta_1 - \theta_2$ pairs which result in the spectra containing $E_3 \sim 0$ or $E_{1-3}^{rel} \sim 0$, and hoped to be able to exclude in the analysis these competitive reactions which, as it should be noted, do not cause difficulties in the $^2H(p,pn)p$ reaction study.

## III. EXPERIMENTAL PROCEDURE

The 156 MeV proton beam extracted in a stochastic manner from the Orsay synchrocyclotron has been used. The liquid deuterium and hydrogen targets used in the first series of experiments are identical to those described in the Ref. 15. Those used in the second series were flat targets of 4 mm thickness and diameter = 35 mm, in order to reduce the energy loss and the straggling effects on low energy outgoing protons. The hydrogen targets were used to calibrate and to check the experimental conditions. The characteristics and the geometrical conditions of the two series of experiments are presented in Table II.

The main modifications in the second series, in addition to the use of a thinner target are (1) the replacement of the plastic scintillation counter $S_1$ by a surface-barrier Si detector of 1000 μm thickness to obtain better energy resolution in $\Delta E_1$, and (2) the use of a ring type plastic scintillation counter after the collimation of telescope 1 coupled in anticoincidence with the NaI detector to minimize edge effects due to the collimation.

The block diagram of the electronics system is

TABLE II. The characteristics and the geometrical conditions of the experimental setup.

| Series | Target (liquid) | Channel 1 (proton 1 at $\theta_1$) Telescope 1 $S_1(\Delta E_1)$ | Channel 1 (proton 1 at $\theta_1$) Telescope 1 NaI($E_1$) | Channel 2 (proton 2 or neutron at $\theta_2$) Telescope 2 $S_2(\Delta E_2)$ | Channel 2 (proton 2 or neutron at $\theta_2$) Telescope 2 Ne 213 |
|---|---|---|---|---|---|
| 1 | Havar wall<br>$\phi$ = 18 mm<br>$L$ = 60 mm | Plastic scintillator (SP 168)<br>$L$ = 41 mm<br>$H$ = 48 mm<br>thick. = 0.5 mm<br>$r$ = 122 cm [a] | $\phi$ = 51 mm<br>$L$ = 76 mm<br>Window<br>Be 0.2 mm<br>Collimator<br>$\phi$ = 40 mm<br>$r$ = 136 cm<br>$\Delta\Omega_1 = 6.91\times10^{-4}$ sr | Plastic scintillator (SP 168)<br>$\phi$ = 175 mm<br>thick. = 2 mm<br>$r$ = 658.5 cm | Liquid scintillator<br>$\phi$ = 175 mm<br>$L$ = 254 mm<br>Window<br>Stainless steel<br>175 $\mu$m<br>$r_2$ = 662.3 cm<br>$\Delta\Omega_2 = 5.65\times10^{-4}$ sr |
| 2 | Havar window<br>$\phi$ = 35 mm<br>thick. = 4 mm | Si-surface barrier-detector<br>$\phi$ = 19.6 mm<br>($\phi_{eff}$ = 18 mm)<br>(surface 300 mm$^2$)<br>thick. = 1000 $\mu$m<br>$r$ = 60 cm<br>A ring plastic scintillator counter is placed in front of the Si detector. | *ibid.* | *ibid.* | *ibid.* |

[a] All $r$ are distances from the reaction chamber center.

presented in Fig. 3. Protons scattered at the angle $\theta_1$ were detected by telescope 1. The fast output of the $S_1$ has been used as a time signal after passing through a constant fraction timing circuit. This time signal was placed in coincidence with the NaI fast output signal and used as a reference for the time of flight of the correlated nucleons entering into channel 2. The time resolution of telescope 1 was of the order of a few ns.

The second telescope was composed of a plastic scintillation counter $S_2$ and a liquid NE 213 scintillation counter. The liquid scintillation counter has been specially designed for the experiment to provide good efficiency for high energy neutrons (~25% for $E_n$ = 70 MeV), and to discriminate against the large $\gamma$ ray background in the experimental room. The details of the construction of this counter and the neutron-$\gamma$ discrimination have

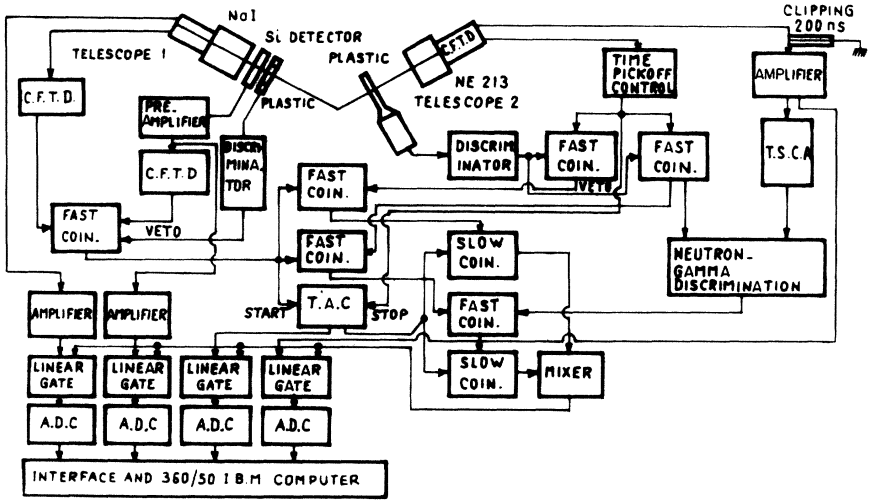


FIG. 3. Block diagram of the experimental setup. The following abbreviations are used: C.F.T.D., Constant Fraction Timing Discriminator; T.S.C.A., Time Single Channel Analyzer; T.A.C., Time to Pulse Height Converter; ADC, Analog to Digital Converter.

been published.[18] This telescope detected charged particles when $S_2$ and the NE 213 counter were coupled in coincidence, and neutrons and $\gamma$ rays when they were coupled in anticoincidence. The $\gamma$ rays were then eliminated by the neutron-$\gamma$ discrimination. Therefore with telescope 2 we can simultaneously detect protons (coincidence events) and neutrons (anticoincidence events).

The fast outputs of telescopes 1 and 2 are fed into a time-to-amplitude converter (TAC). The output amplitude $T$ which is proportional to the difference in flight times between the two channels determines the second nucleon energy $E_2$. Telescope 1 also provides information about $\Delta E_1$ and $E_1$ from their linear output amplitudes. The correlation between $\Delta E_1$ and $E_1$ was used to identify the proper charged particles entering into the channel.

To identify a $(p, 2p)$ or $(p, pn)$ event three independent parameters $\theta_1$, $\theta_2$, and $E_1$ are sufficient, but in order to eliminate completely other competitive reactions we have registered on line the four correlated parameters $E_1$, $\Delta E_1$, $T$, and $E_2$, using a 360-50 IBM computer.

## IV. EXPERIMENTAL DATA TREATMENT AND EXPERIMENTAL RESULTS

The biparametric $E_1$-$T$ events registered and classified on the IBM 360-50 computer were converted into biparametric $E_1$-$T$ spectra using a program. This program includes the choice of the time interval $T \pm \Delta T$ of the $E_1$-$T$ spectra, the subtraction of the accidental and background counts, the conversion of the $E_1$ represented by the channel number to the $E_1$ in MeV, the correction for the tail due to nuclear interactions in the NaI detector, the correction for the neutron counter efficiency in $(p, pn)$ events, and the calculation of the differential cross sections $d^3\sigma/d\Omega_1 d\Omega_2 dE_1$. The efficiency of our neutron counter has been calculated using a Monte-Carlo method based on the method proposed by Kurz,[19] and modified by Narboni at Orsay. We have modified it further for our purpose.

The experimental differential cross sections $d^3\sigma/d\Omega_1 d\Omega_2 dE_1$ for the $^2$H$(p, 2p)n$ and $^2$H$(p, pn)p$ reactions obtained in the second series of experiments for the quasi-free scattering and the final state interaction studies are presented in Figs. 4(a) to 7(b) (some results obtained in the first series have been previously reported[20]). The experimental spectra for the QFS angle pairs (Figs. 5 and 6) are dominated by the strong QFS peaks which appear at approximately $E_3 = 0$. In addition, as expected, the data show only very small FSI contributions on both sides of the QFS peak (at least two orders of magnitude smaller than QFS peak). The small narrow peak at the top of the QFS peak in the $^1$H$(p, p)^1$H spectra (labeled $p$-H) arise from $p$-H elastic scattering due to target impurities. This impurity gives the apparent peaks of 6.3 and 6.0 mb sr$^{-2}$ MeV$^{-1}$, respectively, for the two QFS spectra [Figs. 4(a) and 5(b)] while the true peaks coming from $^2$H$(p, 2p)n$ reaction are evaluated by interpolation from neighboring points as 5.4 and 4.6 mb sr$^{-2}$ MeV$^{-1}$. From these curves, the hydrogen impurity amount in the deuterium target is estimated to be smaller than 2%.

The experimental spectra obtained with the $\theta_1 - \theta_2$ pairs for the FSI in the $^2$H$(p, 2p)n$ reaction show a peak at an energy of $E_1 \sim 30$ MeV [Figs. 6(a) and 7(a)], indicating the effect of the singlet $S$ state of the deuteron due to the $p$-$n$ final state interaction. Similarly, in the $^2$H$(p, pn)p$ reaction [Figs. 6(b) and 7(b)] one observes a double peak with a minimum occurring at $E_1 \sim 30$ MeV, indicating the effect of the Coulomb field in the $p$-$p$ final state interaction. The peaks in the latter case appear at the $E_1$ values corresponding to $E_{1-3}^{\text{rel}} \sim 0,4$ MeV which is the energy of the scattering state of the diproton. In addition, at those FSI angle pairs one again observes the QFS type peak at an $E_1$ energy of about 80 to 90 MeV. The apparent peaks in the spectra of Figs. 6 and 7 at the upper limits of $E_1$ result from the increasing FSI between the second and third nucleons coupled with the cutoff of the spectrum by the kinematic limitations. Finally the peaks in these spectra labeled $p$ and $d$ arise from the $p$-$d$ elastic scattering events as discussed in Sec. II.

The peak values of the experimental differential cross sections $d^3\sigma_{\text{exp}}$ for the $(p, 2p)$ and $(p, pn)$ reactions in each spectrum are summarized in Table III for all measured $\theta_1 - \theta_2$ pairs. The results for the intermediate scattering conditions are not presented in the table but are available upon request. In the same table, we have also presented the ratios $d^3\sigma_{\text{exp}}/d^3\sigma_{\text{SM}}$, $(d^3\sigma_{p,pn}/d^3\sigma_{p,2p})_{\text{exp}}$, and $(d\sigma/d\Omega)_{p-n}^{\text{c.m.}}/(d\sigma/d\Omega)_{p-p}^{\text{c.m.}}$ at the peaks.

To measure background counts, a series of measurements was done using an empty target and the angle pairs employed in the present experiment. The measurement was done with the same proton beam intensity (1 nA) for the same charge unit accumulated in an integrator as in a series of real experiments ($7\,000 \times 10^{-9}$ C). The integrator was connected to a He ionization chamber checked previously by a Faraday cage.

As an example, for the angle pair $\theta_1 = 42.5°$ and $\theta_2 = -45°$, the total number of events registered as correlated proton-proton is 650 and that for proton-neutron is 450 while the corresponding numbers with a liquid hydrogen target are 1.72

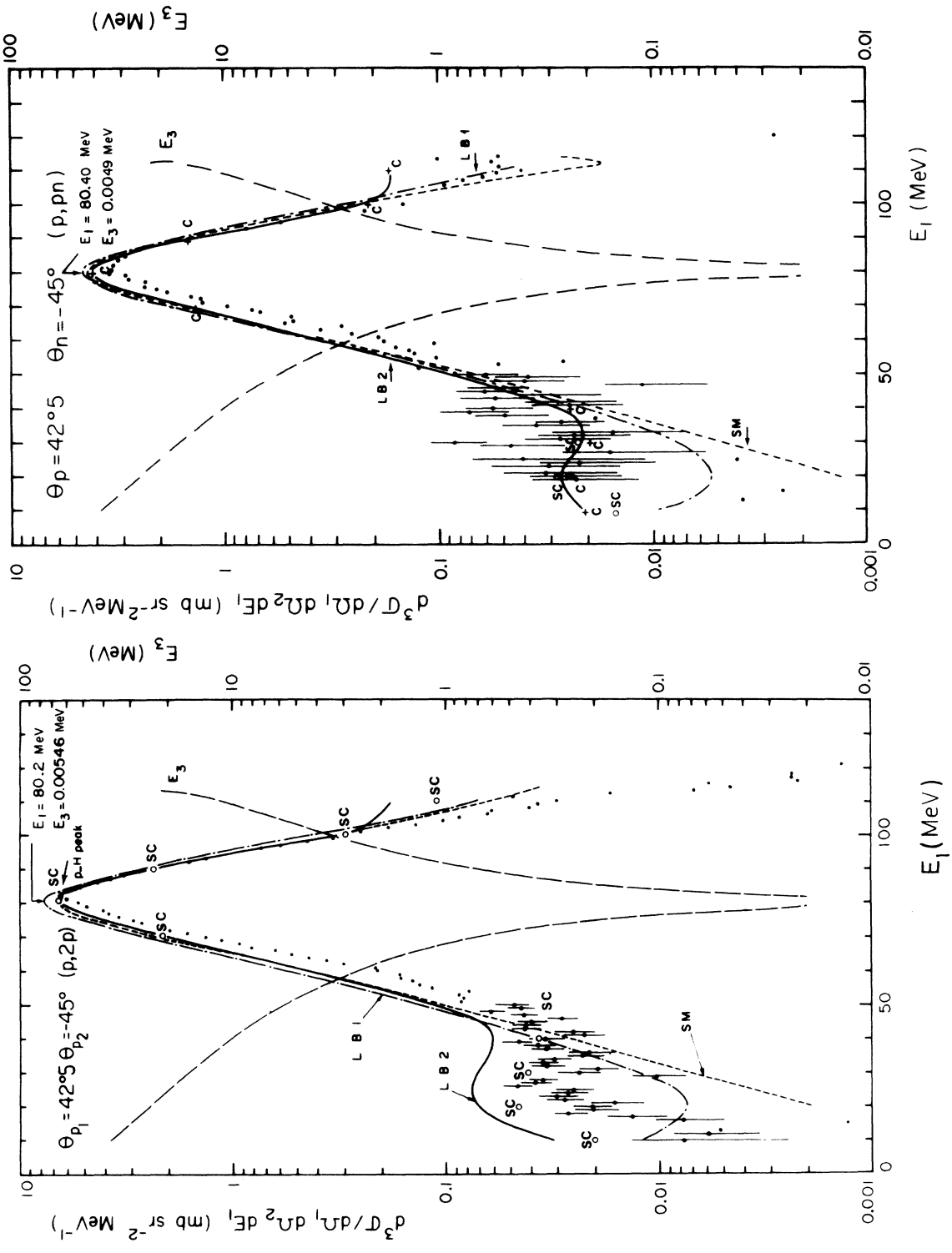


FIG. 4. Experimental QFS $d^3\sigma/d\Omega_1 d\Omega_2 dE_1$ differential cross section spectra with $\theta_1 = 42.5°$ and $\theta_2 = -45°$; (a) $-(p, 2p)$; (b) $-(p, pn)$. The following theoretical curves are also shown: SM, Spectator Model ---; LB1, L'Huillier and Ballot (first order) — - — - —; LB2, L'Huillier and Ballot (first order and second order) ——. Other symbols are defined in the text.

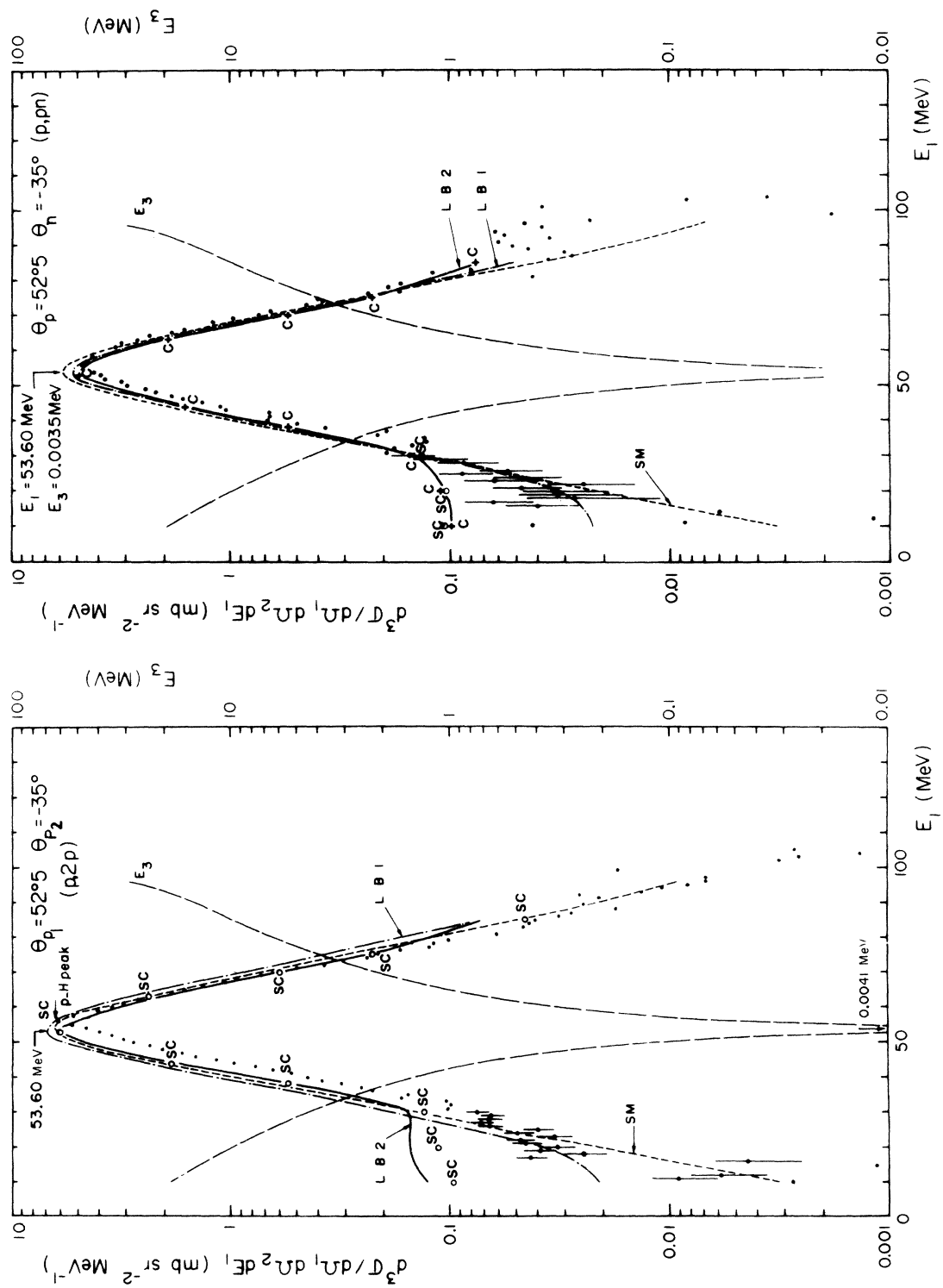


FIG. 5. The QFS $d^3\sigma$ spectra with $\theta_1 = 52.5°$ and $\theta_2 = -35°$; (a) $(p, 2p)$; (b) $(p, pn)$. Other symbols as given in Fig. 4 caption and in the text.

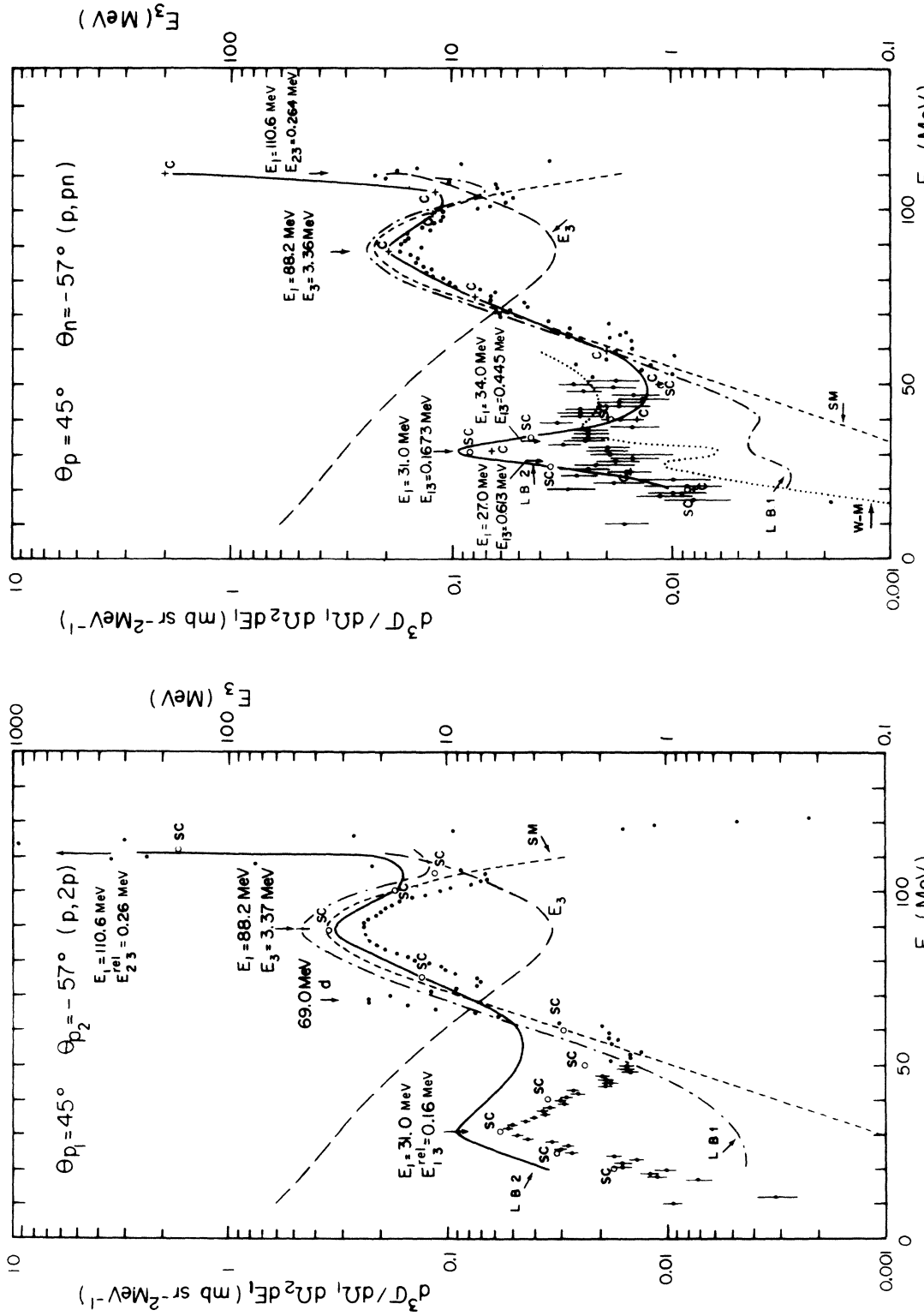


FIG. 6. The FSI $d^3\sigma$ spectra with $\theta_1=45°$ and $\theta_2=-57°$; (a) $(p, 2p)$; (b) $(p, pn)$. Other symbols as given in Fig. 4 caption and in the text.

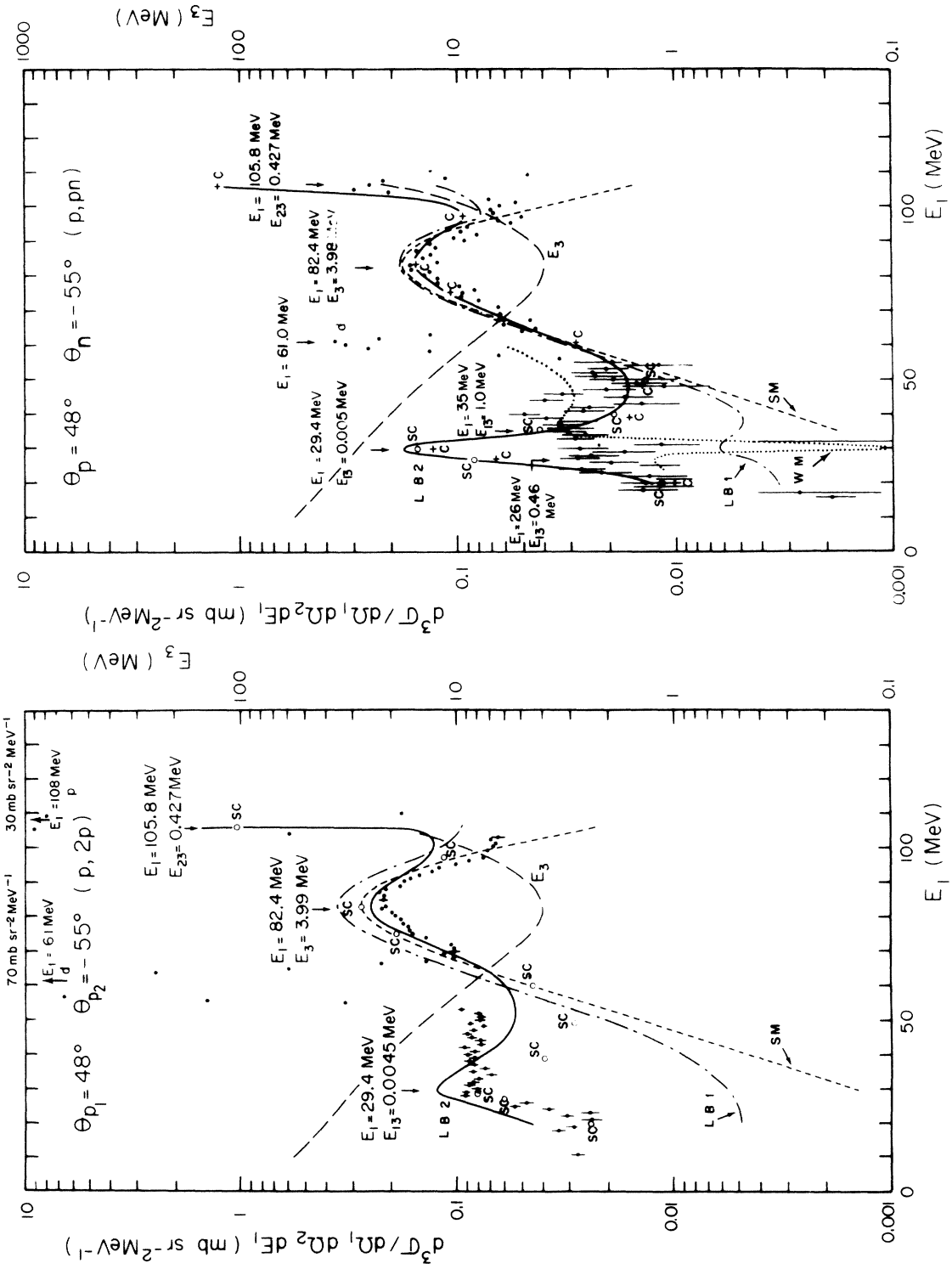


FIG. 7. The FSI $d^3\sigma$ spectra with $\theta_1 = 48°$ and $\theta_2 = -55°$; (a) $(p, 2p)$; (b) $(p, pn)$. Other symbols as given in Fig. 4 caption and in the text.

TABLE III. Kinematical conditions and differential cross sections for the spectral peaks.

| $\theta_1$ (deg) | $\theta_2$ (deg) | Experimental series | $(p, 2p)$ peaks $d^3\sigma_{exp}$ (mb sr$^{-2}$ MeV$^{-1}$) | $\frac{d^3\sigma_{exp}}{d^3\sigma_{SM}}$ | $(p, pn)$ peaks $d^3\sigma_{exp}$ (mb sr$^{-2}$ MeV$^{-1}$) | $\frac{d^3\sigma_{exp}}{d^3\sigma_{SM}}$ | $\left(\frac{d^3\sigma_{p,pn}}{d^3\sigma_{p,2p}}\right)_{exp}$ | $\frac{(d\sigma)_{lab\ p-n}}{(d\sigma)_{lab\ p-p}}$ |
|---|---|---|---|---|---|---|---|---|
| **(1) Quasi-free scattering spectra** | | | | | | | | |
| 42.5 | −45 | 1 | 5.40 ± 0.20 [a] | 0.819 ± 0.030 | 3.06 ± 0.30 | 0.700 ± 0.070 | 0.57 ± 0.05 | 0.665 |
| | | 2 | 5.50 ± 0.20 | 0.835 ± 0.030 | 3.30 ± 0.20 | 0.755 ± 0.045 | 0.60 ± 0.05 | |
| | | Ref. 15 | 5.52 ± 0.30 [b] | | | | | |
| 52.5 | −35 | 1 | 4.40 ± 0.20 [a] | 0.695 ± 0.030 | 4.30 ± 0.31 | 0.740 ± 0.050 | 0.98 ± 0.12 | 0.919 |
| | | 2 | 4.60 ± 0.30 | 0.725 ± 0.045 | 4.50 ± 0.30 | 0.773 ± 0.035 | 0.98 ± 0.13 | |
| | | Ref. 15 | 4.50 ± 0.20 [b] | | | | | |
| **(2) Strong $p$-$n$ and $p$-$p$ final state interaction spectra** | | | | | | | | |
| 45 | −55 | 1 | 0.43 ± 0.01 | 0.724 ± 0.020 | 0.31 ± 0.01 | 0.820 ± 0.025 | 0.72 ± 0.02 | 0.630 |
| 45 | −57 | 2 | 0.26 ± 0.01 | 0.714 ± 0.025 | 0.17 ± 0.02 | 0.720 ± 0.090 | 0.62 ± 0.11 | 0.626 |
| 48 | −55 | 2 | 0.23 ± 0.02 | 0.834 ± 0.070 | 0.16 ± 0.02 | 0.919 ± 0.109 | 0.71 ± 0.15 | 0.644 |

[a] The quasi-free scattering peaks are masked a little by the proton-hydrogen scatterings.
[b] The underlined values are the values obtained in our previous experiments.

$\times 10^6$ and $9 \times 10^3$, respectively. These background events are distributed in 256 channel $\times$ 128 channel matrices in the biparametric $E_1$-$T$ spectra giving almost zero events per matrix cell, that is to say giving quite negligible contribution.

## V. COMPARISON OF EXPERIMENTAL RESULTS WITH THEORETICAL CALCULATIONS

### Spectator-model calculation

The differential cross sections $(d^3\sigma/d\Omega_1 d\Omega_2 dE_1)_{SM}$ have been calculated using the spectator model. The necessary elastic scattering cross sections for the nucleons 1 and 2 were obtained from experimental results. For the $p$-$p$ scattering cross sections $(d\sigma/d\Omega)^{c.m.}_{p-p}$ we have used the current empirical formula of Barashenkov, Maltsec, and Fortschi.[21] For $(d\sigma/d\Omega)^{c.m.}_{p-n}$, we have established the following empirical formula by fitting the experimental cross sections for the $p$-$n$ obtained by Palmieri and Wolfe[22] at an incident energy of 155 MeV:

$$\left(\frac{d\sigma}{d\Omega}\right)^{c.m.}_{p-n} = 3.2\theta_{c.m.,R}{}^2 - 8.3\theta_{c.m.,R} + 7.7,$$

where $\theta_{c.m.,R}$ is the proton scattering angle in the center of mass system in units of radians.

A Hulthên type wave function[23] without the inclusion of the $D$ state was used for the deuteron. In this case, the spectator-model three-body cross section is given by

$$\frac{d^3\sigma}{d\Omega_1 d\Omega_2 dE_1} = \frac{4\sqrt{2}}{\pi^2} \frac{\sqrt{E_\alpha E_\beta}(\sqrt{E_\alpha}+\sqrt{E_\beta})^3}{(E_\alpha+2E_3)^2(E_\beta+2E_3)^2} \frac{\sqrt{E_1}E_2}{\sqrt{E_0}(2\sqrt{E_2}-\sqrt{E_0}\cos\theta_2+\sqrt{E_1}\cos(\theta_1-\theta_2)} \left(\frac{d\sigma}{d\Omega}\right)^{c.m.}_{N-N}$$

where $E_\alpha = 2.226$ MeV and $E_\beta = 59.8$ MeV, and $E_0$, $E_1$, $E_2$, and $E_3$ are the kinematic energies of the incident proton and the scattered nucleons in the laboratory system. For $(d\sigma/d\Omega)^{c.m.}_{p-p}$ we have used the 90° c.m. cross section corresponding to the initial relative energy $(\hbar^2/m)[\frac{1}{2}(\vec{P}_0+\vec{P}_3)]^2$ where $\vec{P}_0$ and $\vec{P}_3$ are the incident and recoil momenta, respectively. For $(d\sigma/d\Omega)^{c.m.}_{p-n}$ we have used the same incident energy prescription and an angle which corresponds to the proton scattering angle in the two-body center of mass system. The latter is exact only in the relative energy region of 154/2 MeV, and if $E_3$ becomes large, the validity decreases. However, we present the $d^3\sigma_{SM}$ only to give a rough idea of the general form of the spectra in the QFS region. The results of these calculations are plotted in the Figs. 4(a) to 7(b) as a fine broken line and marked SM.

We should point out that the ratio $d^3\sigma_{exp}/d^3\sigma_{SM}$ at the QFS peak does not always have the same

value when kinematic conditions are changed. The ratio $(d^3\sigma_{p,pn}/d^3\sigma_{p,2p})_{exp}$ is approximately the same as the ratio of the elastic scattering cross sections for the interaction $p$-$n$ and $p$-$p$, $(d\sigma)_{p-n}/(d\sigma)_{p-p}$. These facts suggest two things, namely, in the quasi-free peak, the primary scattering is dominant, and the ratio $(d^3\sigma_{p,pn}/d^3\sigma_{p,2p})$ depends not only on the incident energy[24] but also on the scattering angle.

### Calculations of L'Huillier and Ballot

L'Huillier and Ballot have calculated the $d^3\sigma$ which correspond to our kinematic conditions. Their expression for the differential cross sections $d^3\sigma_{LB}$ can be presented in the following form:

$$\frac{d^3\sigma}{d\Omega_1 d\Omega_2 dE_1} = \left(\frac{2\pi}{h}\right)^4 \frac{m^2}{4} K^{inel} |t_{fi}^{inel}|^2 , \quad (1)$$

where $K^{inel}$ is a relativistic kinematic factor.

The scattering matrix element for three nucleons $t_{fi}^{inel}$ can be represented by a nucleon-nucleon multiple scattering series. They have used, for the present calculation, the potentials of Hamada-Johnston (hard core) and Sprung-de Tourreil (super soft core) (SSC).[25] In order to calculate the second order scattering, L'Huillier and Ballot have factorized the primary interaction by assuming that the scattered nucleon was at rest in the deuteron. Their two nucleon scatterings include off-energy effects, but the Coulomb interaction is excluded. The details of the calculation are described in the thesis of L'Huillier.

The calculated $d^3\sigma$ are plotted in the Figs. 4(a) through 7(b) with the dashed-dot line for the first order calculations (labeled LB1) and with the continuous line for the first plus second order calculations (labeled LB2). The experimental $d^3\sigma$ agrees better with the LB2 than LB1, indicating the necessity of including the second order interaction in the calculation, even in the QFS regions (Figs. 4 and 5). The inclusion of the second order terms gives tremendous improvement in the FSI regions (Figs. 6 and 7), as one might expect. However, there is always some disagreement between the $d^3\sigma_{exp}$ and $d^3\sigma_{LB2}$, even in the QFS peak. This disagreement could be sensitive to the choice of the nucleon-nucleon potential (if the notion of this model is valid). But the Hamada-Johnston potential and that of Sprung-de Tourreil do not show any significant differences in the quasi-free scattering peaks when calculated to second order.

The QFS peak ratios $d^3\sigma_{exp}/d^3\sigma_{LB2}$ are about 0.80 for the $(p,2p)$ and $(p,pn)$ reactions at both the $(52.5°,-35°)$ and the $(42.5°,-45°)$ angle pairs. The peak ratio $(d^3\sigma_{p,pn}/d^3\sigma_{p,2p})_{LB2}$ is 0.84 for the first angle pair and 0.63 for the second one, indicating that this ratio depends on the scattering angle.

The $d^3\sigma_{exp}$ for the FSI peak regions in the $(p,2p)$ reaction for the $(45°,-57°)$ pair are smaller than those calculated with the first plus second order interaction using all partial waves (LB2). However, it is interesting that these FSI data are accidentally in good agreement with the $d^3\sigma$ calculated by neglecting the $D$ state of the deuteron and by using only $s$ waves in the final state interaction. These simplified calculations are indicated in Figs. 6(a) and 7(a) by open circles and labeled by SC. This tendency is seen also for the FSI peak in the $(p,2p)$ reaction at the $(48°,-55°)$ pair, but in this case the strong deuteron peak reaction tail from the NaI crystal, due to the $p$-$d$ elastic scattering, covers one part of the FSI peak. The "deuteron tail" contributions to the cross section are of the same order of magnitude as the FSI contributions at $E_1 \sim 30$ MeV.

The $d^3\sigma_{exp}$ for the FSI peak in the $(p,pn)$ reaction cannot be explained by the calculation of L'Huillier and Ballot since it does not contain the Coulomb field. The $p$-$p$ FSI peak must be strongly influenced by the Coulomb field, since the minimum relative energy between two protons $E_{1-3}^{rel}$ is small in these cases—0.160 and 0.0052 MeV—for the $(45°,-57°)$ and $(48°,-55°)$ pairs, respectively. This Coulomb effect is clearly shown in the experimental data by the minimum in the FSI peak [Figs. 6(b) and 7(b)], as has already been mentioned in Sec. IV. The differential cross sections calculated by L'Huillier and Ballot for the $(p,pn)$ reaction with a central potential and with $s$ waves only (SC) fit the experimental data fairly well, except in the FSI region ($E_{1-3}^{rel} \sim 0$), where the calculation shows a peak.

### Calculations of Sakamoto and Takeutchi

Formerly Sakamoto, Takeutchi, and Yuasa have examined the role of the Coulomb force in the calculation of the final state interaction for the $^2H(p,2p)n$ reaction.[14] Sakamoto and Takeutchi have extended the calculations to the $^2H(p,pn)p$ reaction.[26]

The essential differences between the L'Huillier-Ballot calculations and the Sakamoto-Takeutchi calculations, both of them being performed with the Hamada-Johnston potential, are due to the treatment of the intermediate interaction and the effects of the Coulomb field. L'Huillier and Ballot obtained the factorization to calculate the first and second order interactions by using a constant value for the struck nucleon momentum $\vec{k}$ in the primary scattering. Sakamoto and Takeutchi,

on the other hand, have calculated the $t$ matrices by using $\vec{k} = -\vec{k}_t$ for the struck nucleon to calculate the relative energy between two nucleons in the primary interaction and by using the final relative energy in the second interaction. They have solved the Schrödinger equation with the Hamada-Johnston potential including the Coulomb force in order to obtain the quantities needed for the numerical calculations.

The cross sections $d^3\sigma_{ST}$ are generally in good agreement with $d^3\sigma_{LB2}$ for the quasi-free peak regions in the $^2H(p, 2p)n$ and $^2H(p, pn)p$ reactions, but do not agree in the final state interaction regions of either reaction. The former calculation is, in general, smaller than the latter, even without the Coulomb force. Generally speaking, the $d^3\sigma_{ST}$ in the FSI region of the $^2H(p, pn)p$ is of the same order of magnitude as $d^3\sigma_{LB1}$, and about a factor of 6 smaller than the $d^3\sigma_{exp}$.

The calculations of Sakamoto and Takeutchi are some of the first which include the Coulomb force at an incident energy higher than 100 MeV, and they clearly produce a minimum $d^3\sigma$ at the smallest relative energy between the two protons.

### Calculations of Wallace

Wallace has extended his previously published calculation (Ref. 6) to 156 MeV. His method is a modification of the calculation in which the exact three-body Faddeev equations are solved with an approximate, separable two-nucleon interaction. In his model, the spin dependent, $s$-wave, separable, two-nucleon scattering amplitude is modified to fit the on-shell two-nucleon elastic scattering data at energies above 20 MeV. The coupled integral equations for the model three-nucleon system are solved iteratively, so that the Faddeev-Watson nuclear multiple scattering series is generated.

The difficulty at higher energies arises from the fact that the separable two-body interactions usually employed cease to provide a realistic description of the observed two-nucleon processes. Wallace uses as input a one-term separable two-nucleon $t$ matrix which reduces at lower energies to the $t$ matrix obtained from the Yamaguchi $s$-wave potential. This $t$ matrix might not be unreasonable as it has the correct magnitude on the energy shell, and the on-shell point is heavily weighted in the three-body equations at higher energies. The two-body $t$ matrices used in the present calculations have been fitted to reproduce the energy dependence of $(d\sigma)^{c.m.}_{p-p}(90°)$ and $(d\sigma)^{c.m.}_{p-n}(90°)$. No Coulomb interaction has been included here.

The first order contribution is essentially the same as the spectator model term in the QFS region, since the nucleon-nucleon $t$ matrix is fitted to the on-shell data. However, the complete multiple scattering calculation includes contributions from all higher order scattering processes, which depend on completely off-energy-shell two-body $t$ matrices. The $d^3\sigma$ for single scattering, single + double scattering, single + double + triple scattering, and the exact solution have been also obtained.

In the Wallace calculations, the single plus double scattering contribution gives the best fit to the experimental data, while the complete multiple scattering series calculation produces a very small cross section in the FSI region. Such dramatic behavior resulting from the higher order terms may question the convergence of the multiple scattering series with one-term separable two-nucleon $t$ matrix at our energy.

### Enhancement factor of Watson-Migdal

We have tried to see if the Watson-Migdal enhancement factor could explain the final state $p$-$p$ interaction peak (or valley) in the region where $E^{rel}_{1-3} \sim 0$. It is a simple calculation including the Coulomb interaction when compared to the difficulty of introducing correctly the Coulomb field into an off-energy shell two-nucleon interaction. The formulas used to calculate this factor are the same as given in Ref. 27. We have used the following nucleon-nucleon interaction parameters[27] in our calculation:

$$a_{pp} = -7.67 \text{ fm}, \quad a_{np} = -23.73 \text{ fm}, \text{ and } r_0 = 2.7 \text{ fm}.$$

The calculated Watson-Migdal factor was multiplied by $d^3\sigma_{SM}$.

The results are shown as the fine dotted curve in the Figs. 6(b) and 7(b). The positions of the maxima and minima of the spectra are correctly reproduced, but the shape and the absolute cross section do not fit the experimental results. In reality it would be better to use $d^3\sigma_{LB1}$ in place of $d^3\sigma_{SM}$ in order to judge the validity of the Watson-Migdal enhancement factor. However, the calculation does show the general features expected for the FSI, and one does not expect the validity of the formula to extend beyond about $E^{rel}_{1-3} \gtrsim 2$ MeV which corresponds to $E_1 \sim 40$ MeV in our FSI kinematic conditions.

## VI. CONCLUSION

The experimental cross-section spectra, $d^3\sigma_{exp}$, as a function of a proton energy have been obtained for the $^2H(p, 2p)n$ and $^2H(p, pn)p$ reactions at 156 MeV. Various angle pairs were chosen covering quasi-free and final state interaction kinematic

conditions as well as some other intermediate cases.

These experimental results show that: (1) near the QFS peak the $^2H(p,2p)n$ and the $^2H(p,pn)p$ reactions at 156 MeV are dominated by the simple scattering, but also that the contribution coming from multiple scattering effects are not negligible; (2) the ratio $d^3\sigma_{p,pn}/d^3\sigma_{p,2p}$ at the QFS peak is angular dependent; (3) the $p$-$n$ and $p$-$p$ final state interactions are present when a very small relative energy $E^{rel}_{p-n}$ or $E^{rel}_{p-p}$ is permitted. The cross section corresponding to the $p$-$p$ FSI shows a minimum when $E^{rel}_{p-p} \sim$ zero and a maximum when $E^{rel}_{p-p} \sim 0,4$ MeV, indicating the presence of the Coulomb interaction. The cross section corresponding to the $p$-$n$ FSI shows a maximum when $E^{rel}_{p-n} \sim 0$.

We have compared our experimental cross sections with several theoretical calculations in the framework of the approximate Faddeev solutions; i.e., calculations of (1) L'Huillier and Ballot, (2) Sakamoto and Takeutchi, and (3) Wallace. The first explains the $^2H(p,2p)n$ reaction fairly well in all regions, but does not fit the $(p,pn)$ data in the FSI region since the Coulomb interaction was not taken into account. The second also explains fairly well the $(p,2p)$ reaction in the QFS and FSI peak regions indicating that the off-energy shell interaction effect is not very important in these regions. However, the differences between the first and second calculation are large in the intermediate regions. The Coulomb interaction in the $p$-$p$ FSI is explained qualitatively in the second calculation but the calculated $d^3\sigma$ is much too small. The third calculation explains $d^3\sigma_{exp}$ in the FSI region of the $(p,2p)$ reaction when the multiple scattering series is limited to the first and second terms. The fit becomes worse when the full multiple scattering series is considered.

The comparison of the $d^3\sigma_{exp}$ and $d^3\sigma_{th}$ indicates that the development of the three-nucleon scattering amplitude in a multiple scattering series of the two-nucleon scattering amplitudes, taking into account first and second order terms, and using a realistic potential might be more adequate to describe the deuteron breakup process at intermediate energy than a calculation including the full multiple scattering series but limited to the $S$-wave contribution. To understand this behavior, the multiple scattering mechanism should be studied more extensively with very realistic potentials in a more complete Amado type calculation. The introduction of Coulomb interaction in any case remains somewhat problematic.

## ACKNOWLEDGMENTS

The authors are grateful to Professor Benoist-Gueutal, Dr. Ballot, and Dr. L'Huillier for valuable discussions; in particular, Dr. L'Huillier permitted us to use her cross sections calculated for our kinematic conditions. Dr. Wallace, Dr. Sakamoto, and Dr. Takeutchi have also undertaken the calculations for our kinematic conditions. All of them are very much thanked. The authors wish to thank Mr. Debray and the staff of the synchrocyclotron of Orsay, Mr. Buhler, and Mr. Mommejat and the members of the Cryogenic section for liquid targets, Dr. Picard, Mr. Brun, and Mr. Jory of the 360 IBM computer section for on-line registration, and Mr. Camon and the design center staff for the construction of detectors. The assistance of Mrs. Rouvet and Mrs. Marchal for the analysis of the experimental results are very much appreciated. We thank very much Professor P. G. Roos for reading the manuscript and offering suggestions.

---

*On leave from the Institute of Physics, University of San Paul, San Paul, Brazil.

†On leave from the University of Liban, Hadat-Beyrouth, Liban.

‡On leave from the Tokyo Institute of Technology, Meguro, Tokyo, Japan.

[1]L. D. Faddeev, Zh. Eksp. i Teor. Fiz. 39, 1459 (1960) [transl.: Sov. Phys. JETP 12, 1014 (1961)]; C. Lovelace, Phys. Rev. 135, B1225 (1964).

[2]R. Aaron, R. D. Amado, and Y. Y. Yam, Rev. Mod. Phys. 37, 516 (1965); R. Aaron and R. D. Amado, Phys. Rev. 150, 857 (1966).

[3]I. H. Sloan, Phys. Rev. 185, 1361 (1969); Nucl. Phys. A168, 211 (1971); R. T. Cahill and I. H. Sloan, 165, 161 (1971).

[4]Y. Avishai, W. Ebenhöhe, and A. S. Rinat-Reiner, Ann. Phys. (N. Y.) 55, 341 (1969).

[5]M. Durand, Ph.D. thesis, Grenoble, 1972 (unpublished).

[6]J. M. Wallace, Phys. Rev. C 7, 10 (1973); private communication.

[7]G. F. Chew, Phys. Rev. 80, 196 (1950); Phys. Rev. 84, 710 (1951).

[8]G. F. Chew and G. C. Wick, Phys. Rev. 85, 636 (1952).

[9]A. Everett, Phys. Rev. 126, 831 (1962).

[10]A. Cromer, Phys. Rev. 129, 1680 (1963); A. Cromer and E. H. Thorndike, Phys. Rev. 131, 1680 (1963).

[11]P. Benoist-Gueutal and F. Gomez-Gimeno, Phys. Lett. 13, 68 (1965); J. Phys. 26, 403 (1965).

[12]M. L'Huillier, Nucl. Phys. A129, 196 (1969).

[13]C. N. Brown and E. H. Thorndike, Phys. Rev. 177, 2067 (1969); C. N. Brown, Ph.D. thesis, University of Rochester, 1968 (unpublished).

[14]F. Takeutchi, Y. Sakamoto, and T. Yuasa, Phys. Lett. 35B, 198 (1971); Proceedings of the Symposium of the Nuclear Three-Body Problem and Related Topics, Budapest, July, 1971 (unpublished), p. A-6; F. Takeutchi and Y. Sakamoto, Nucl. Phys. A185, 366 (1972).

[15]K. Kuroda, F. Takeutchi, and T. Yuasa, J. Phys. Soc. Jap. Suppl. 24, 76 (1968); F. Takeutchi, T. Yuasa, K. Kuroda, and Y. Sakamoto, Nucl. Phys. A152, 434 (1970); F. Takeutchi, Ph.D. thesis, University of Tokyo, 1971 (unpublished).

[16]M. Morlet, F. Frascaria, B. Geoffrion, N. Marty, and B. Tatischeff, Nucl. Phys. A129, 177 (1969).

[17]M. Morlet, R. Frascaria, N. Marty, and A. Willis, Nucl. Phys. A191, 385 (1972); M. Morlet, Ph.D. thesis, Orsay, 1972 (unpublished).

[18]H. Nakamura, F. Reide, and T. Yuasa, Nucl. Instrum. Methods 108, 509 (1973).

[19]R. J. Kurz, UCRL Report No. 11, 339, 1964 (unpublished).

[20]J. P. Didelez, I. D. Goldman, E. Hourani, H. Nakamura, F. Reide, and T. Yuasa, J. Phys. (Paris) 33, 129 (1972), No. 8, 9; *Proceedings of the International Conference on Few-Particle Problems in the Nuclear Interaction, Los Angeles, August, 1972* (North-Holland, Amsterdam, 1973), p. 483.

[21]V. S. Barashenko and V. M. M. Maltsev, Fortschr. Phys. 9, 549 (1961).

[22]J. N. Palmieri and J. P. Wolfe, Phys. Rev. C 3, 144 (1971).

[23]A. F. Kuckes, R. Wilson, and P. F. Cooper, Jr., Ann. Phys. (N. Y.) 15, 193 (1961).

[24]E. L. Petersen, R. G. Allas, R. O. Bondelid, in *Proceedings of the International Conference on Few-Particle Problems in the Nuclear Interaction, Los Angeles, August, 1972* (see Ref. 20), p. 503.

[25]R. de Tourreil and D. W. L. Sprung, Nucl. Phys. A201, 215 (1973).

[26]F. Takeutchi and Y. Sakamoto, in *Proceedings of the International Conference on Few-Particle Problems in Nuclear Interaction, Los Angeles, 1972* (see Ref. 20), p. 347.

[27]H. Brückmann, W. Gehrke, W. Kluge, H. Mathäy, L. Schâgler, and K. Wick, *Three-Body Problem in Nuclear and Particle Physics* (North-Holland, Amsterdam, 1970), p. 230.